3D-printed electrospinning setup for the preparation of loratadine nanofibers with enhanced physicochemical properties

Rita Ambrus[a], Areen Alshweiat[a], Ildikó Csóka[a], George Ovari[b], Ammar Esmail[b], Norbert Radacsi[b]

[a]Institute of Pharmaceutical Technology and Regulatory Affairs, University of Szeged, Interdisciplinary Excellence Centre, Eötvös u. 6, H-6720 Szeged, Hungary

[b]The School of Engineering, Institute for Materials and Processes, The University of Edinburgh, Robert Stevenson Road, Edinburgh, EH9 3FB, UK

*Correspondence to Norbert Radacsi

The School of Engineering, Institute for Materials and Processes, The University of Edinburgh, Robert Stevenson Road, Edinburgh, EH9 3FB, UK

Tel: +44 131 651 3571

E-mail: n.radacsi@ed.ac.uk

ABSTRACT

This study investigates the effects of drug-loaded nanofibers on the solubility of the poorly water-soluble drug, loratadine. Amorphous morphologies of electrospun loratadine nanofibers were prepared using a 3D-printed electrospinning setup. Polyvinylpyrrolidone was used as a carrier in the solvent preparation method. The prepared nanofibers were characterized by scanning electron microscopy, differential scanning calorimetry, X-ray diffraction analysis, Fourier transform infrared spectroscopy, solubility and in vitro dissolution studies with kinetic behavior evaluation. The scanning electron microscope images showed smooth nanofiber surfaces with a mean diameter of 372 nm. Moreover, both differential scanning calorimetry and X-ray diffraction analysis confirmed the amorphous state of the prepared nanofibers. FT-IR results suggested that loratadine lost its original crystal structure by hydrogen bonding interactions. The fabricated nanofibrous drug samples demonstrated a remarkable 26-fold increase in solubility when compared to the pure drug in phosphate buffer at pH 7.4. Furthermore, dissolution studies showed that 66% of the drug from the nanofibrous mat was released in the first 10 min, which is significantly higher than the maximum of 4% drug release of the reference samples within the same time. Thus, Loratadine nanofibers can be considered as an alternative dosage form with improved physicochemical properties.

Keywords: Electrospinning, 3D printing, Nanofibers, Loratadine, Physicochemical analysis

1. INTRODUCTION

Loratadine (LOR) is a second-generation anti-histamine (H_1) agent. It is frequently prescribed to treat allergic disorders without a central nervous system depressant effects (Simons, 2002).

LOR belongs to class II of the biopharmaceutical classification system that exhibits a poor water solubility (0.00303 mg mL^{-1}) and high permeability (log P of 5) (Dagenais et al., 2009). From the chemical point of view, LOR contains pyridine nitrogen atom that is responsible for its pH-dependent solubility (Han et al., 2004). Its pKa value at 25 ºC has been reported as 4.85–6.00 (Dagenais et al., 2009; Han et al., 2004; Omar et al., 2007). Related to the properties mentioned above, LOR shows low and variable bioavailability (Arya et al., 2012). Many possibilities have been applied to enhance the dissolution and solubility of LOR, which includes solid dispersion, inclusion with ß-cyclodextrin derivatives, micellar solubilization and self-microemulsifying drug systems (Frizon et al., 2013; Li et al., 2015; Nacsa et al., 2009, 2008).

In recent years, many efforts have been devoted to utilizing nanoparticle design for increasing the bioavailability of drugs. Preparation of LOR nanoparticles has been shown to enhance its dissolution and solubility (Alshweiat et al., 2018; Rodriguez Amado et al., 2017). The use of nanoparticles to produce LOR with increased hydrophilic properties shows promise and has opened the scope for new methods of preparation and administrations (Akhgari et al., 2016). Nanofibers, due to their architecture, are considered to be a sophisticated solution to the current inconveniences of drug delivery (Li et al., 2015). Drugs based on nanofibers show faster dissolution kinetics than their micron-sized counterparts, as nanofibers have a significantly higher surface area to volume ratio (Jiang et al., 2004).

Among different method of preparation, electrospinning is considered as the most efficient process in nanofiber production. This process has been recognized as simple and versatile to produce nanofibers with low cost (Huang et al., 2003). Radacsi et al. (Radacsi et al., 2018) reported the benefits of electrospinning on scaling up to high yield. This feature makes electrospinning attractive for the industry over the electrospray technique. Both methods are

based on electrohydrodynamic atomization and have been demonstrated to improve the physicochemical properties of drug particles (Ambrus et al., 2013; Radacsi et al., 2019).

The poor water solubility of the active pharmaceutical ingredients (APIs) and candidates is one of the major challenges of the pharmaceutical industry (Craig, 2002). The delivery of these agents is associated with poor bioavailability (Amidon et al., 1995). As a novel drug manufacturing method, electrospinning is mainly focused on enhancing the dissolution of poorly water-soluble drugs. The enhanced dissolution of drugs in the nanofibers are related to presence of the amorphous state, high specific surface area, increased wettability and solubility, and lower precipitation (Nagy et al., 2012). This offers alternative drug delivery methods, e.g. the electrospun drug films can be used for transdermal delivery, or it can dissolve in the oral cavity (e.g. sublingual or buccal administration), which can be advantageous for patients that cannot swallow (Shahriar et al., 2019). Furthermore, the advanced bioavailability also reduces the side-effects of the drugs (Badawy et al., 1996).

Recently, academic and industrial efforts have concentrated on enhancing the dissolution of the poorly water-soluble pharmaceutical agents by electrospinning technology. The fabrication of itraconazole nanofibers using the co-polymer PVPVA64 as a carrier was done by novel high-speed electrospinning method (Nagy et al., 2015). The produced amorphous nanofibers showed rapid dissolution, 90% of the drug was dissolved within 10 min. The high-speed electrospinning method has a significantly higher production rate than the conventional electrispinning techniques, making it attractive for industrial pharmaceutical manufacturing. In another study, electrospinning of itraconazole was performed with hydroxypropylmethylcellulose as a carrier polymer (Verreck et al., 2003). The authors highlighted the amorphous structure and the rapid and complete dissolution of the API, itraconazole, from the prepared nanofibers.

Electrospinning has been utilized in poorly water-soluble analgesics. Ketoprofen showed a significant dissolution from the prepared nanofibers with PVP K30 as a drug carrier and filament-forming a polymer. The complete drug release was achieved within just 30 min. However, the pure drug showed approximately 5% release after 2 h (Yu et al., 2010). Moreover, niflumic acid loaded nanofibers into PVP (MW = 1,300,000) were incorporated into capsules. The formulations showed a drug release of 69-91% after 15 min (Radacsi et al., 2019). The high drug release from nanofibers was also achieved in acetaminophen. Yu et al (Yu et al., 2010) found that 93.8% of poorly water-soluble acetaminophen was released in the first 2 min from the PVP (Mw=360,000) drug-loaded nanofibers. Furthermore, ibuprofen has been fabricated into nanofibers (Potrč et al., 2015). The nanofibers released 100% of the ibuprofen in 4 h.

To prepare nanofibers of the poorly water-soluble plant sterol. Paaver and co-workers (Paaver et al., 2016) fabricated β-sitosterol loaded chitosan nanofibers. The prepared nanofibers exhibited freely water-soluble properties with a very short lag-time in releasing the β-sitosterol. In a study by Li et al (Li et al., 2013), rapid and improved dissolution rates have been achieved for caffeine and riboflavin nanofibers, using polyvinyl alcohol polymer as filament-forming polymer and drug carrier. The nanofibers showed 100% and 40% release of caffeine and riboflavin, respectively within 60 s.

In comparison to the conventional processes of solid dispersion fabrication, electrospinning can produce nanofibers with enhanced dissolution compared to film casting (Potrč et al., 2015) freeze-drying, vacuum drying, and heating drying (Yu et al., 2010).

Many studies discussed the effects of the material and process parameters of electrospinning on the release of poorly water-soluble drugs from the nanofibers. These parameters include; drug characteristics (Potrč et al., 2015), polymer type (Baskakova et al., 2016), drug and polymer ratios (Brewster et al., 2004), solvents type and ratios (Paaver et al., 2016), in

addition to the electrospinning parameters of voltage (Verreck et al., 2003), and the distance between the collector and the spinneret (Radacsi et al., 2019).

The material properties affect the properties of the solutions, such as viscosity and surface tension thus morphology and size of the electrospun nanofibers (Fong et al., 1999). In general, concentration is a critical factor determining the solution viscosity, whereas polymer and solvent affect the value of the surface tension (Yang et al., 2004). Moreover, adjusting the process parameters has significant effects on controlling the final structure of the electrospun fibers (Ryu et al., 2003).

Polyvinylpyrrolidone (PVP) is a widely used polymer for preparing electrospun fibers. It shows low toxicity, high biocompatibility and excellent solubility in most organic solvents (Chuangchote et al., 2009). Furthermore, PVP with the M_w 1,300,000 g mol^{-1} has been the most thoroughly investigated in reported studies related to electrospinning with PVP (Li and Xia, 2003; Nuansing et al., 2006).

In the present study, a low-cost 3D-printed electrospinning setup is investigated as a new formulation method for the fabrication of nanostructured LOR. From the production point of view, this study considered the first application of a setup prepared by fused deposition modelling printing method with 3D-printed components (Huang and Radacsi, 2019). Concerning the pharmaceutical goal, this study aimed to produce nanofiber with enhanced dissolution and high drug loading of the poorly water-soluble LOR. These properties enable the incorporation of the nanofibers into different dosage form such as oral, buccal, topical, and transdermal with improved bioavailability. The size and morphology of the produced LOR-PVP nanofibers were characterized by scanning electron microscopy. The structure of the products was investigated using differential scanning calorimetry, X-ray powder diffraction and Fourier transform infrared. The solubility and *in vitro* release of the selected

product was studied in a phosphate buffer solution at pH 7.4 and was compared with the corresponding physical mixture and a prepared reference sample.

2. Experimental

2.1 Materials

Loratadine (LOR) was purchased from Teva Ltd. (Budapest, Hungary). Polyvinylpyrrolidone (PVP; M_w 1,300,000 g mol^{-1}) was purchased from Alfa Aesar, UK. 99.99% purity ethanol was obtained from Fisher Scientific, UK.

2.2. Solution preparation and electrospinning

LOR: PVP at 1:1 ratio was used to prepare the electrospinning samples containing PVP as a carrier and ethanol as a solvent system. 0.77 g LOR was mixed with 0.77 g PVP, and this powder mixture was dissolved in 50 mL ethanol. The electrical conductivity of the solution was 2 μS cm^{-1}. This solution was sucked into a 60 mL syringe (BD plastics). The nanofibers were produced in a 3D-printed electrospinning setup (Figure 1). The details of the 3D printing process and the files of the electrospinning setup can be found in another work (Huang and Radacsi, 2019). A 20G needle was applied at the tip of the syringe, and it was placed into the syringe pump (Cole-Parmer, USA). The LOR solution was injected into the 3D-printed chamber through a Teflon tube using the automatic pump with a pumping speed of 15 μL min^{-1}. The Teflon tube (inner diameter 0.8 mm) was connected to a blunt 20G needle that was placed inside the 3D-printed setup and was covered by a safety cap to prevent electric shock. The blunt nozzle was charged by a +35 kV DC high-voltage power supply (Information Unlimited, Amherst, USA) at its maximum voltage. The working distance (*WD*) between the spinneret and the fiber collector was set to either 65 or 95 mm (95 mm was the maximum distance possible in the setup without using extension parts). The fibers were

collected on an 80 mm wide grounded stainless steel drum, which was rotating with a speed of 100 rpm. A constant stream of air (5.2 ms^{-1}) was supplied into the chamber opposing the direction of the electrospun fibers, in order to increase the evaporation rate of the solvent from the electrospun jet and the fibers as they travelled across the chamber. Two different working distances between the injection nozzle and the collection drum were tested in the experiments, and all the other parameters were fixed. The experiments were performed at room temperature at the relative humidity of 42-49%. Each run lasted for 15 minutes.

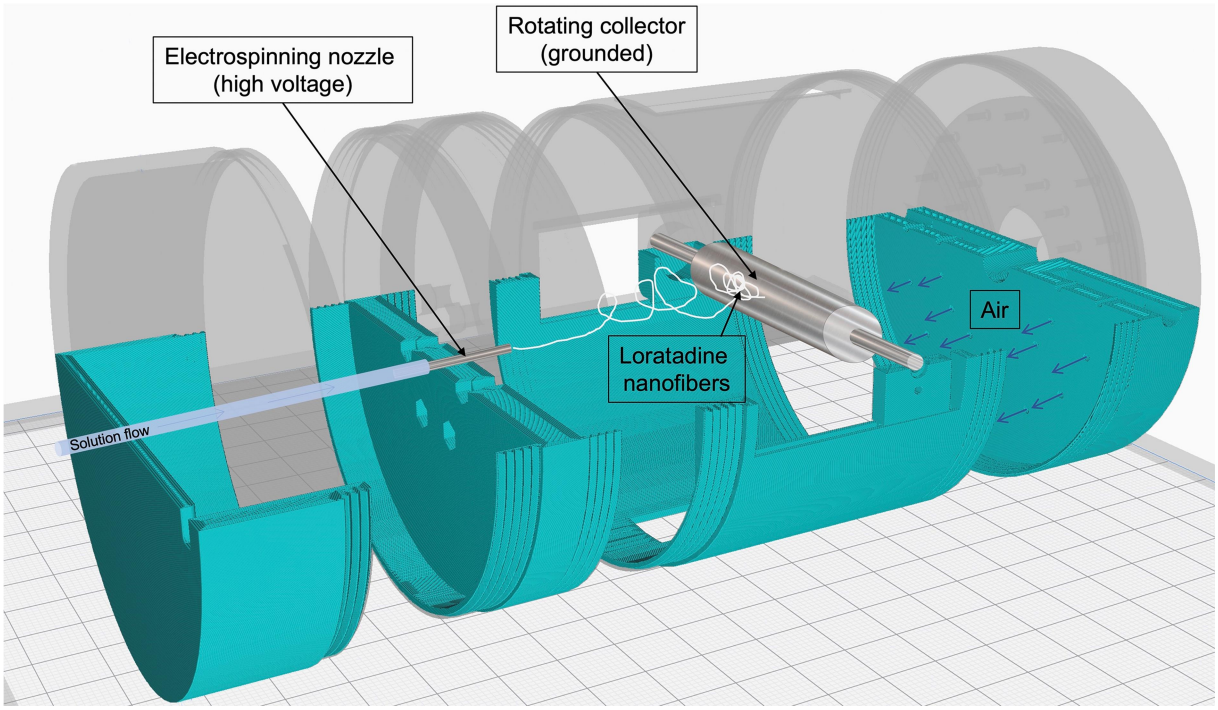

Figure 1. Schematic illustration of the 3D-printed modular electrospinning setup.

2.3 Preparation of the reference samples

The reference samples, physical mixture (PM) and the solvent evaporated sample (SE), were prepared by two different methods to control the effect of polymer and re-crystallization procedure on the physicochemical properties of LOR. In the first method the physical mixture (PM) was prepared by Turbula mixer System (Schatz; Willy A. Bachofen AG Maschinenfabrik, Basel, Switzerland) of LOR and PVP with 1:1 ratio at 50 rpm for 10 min

188 (PM). The second method involved the evaporative re-crystallization of the previously mixed
189 PM which was dissolved in 100 mL ethanol. The solvent was evaporated at 25 ºC. The
190 preparation methods of the nanofibers and reference samples are summarized in Table 1.
191

Table 1. Composition and method of preparation of loratadine nanofibers and reference samples.

Sample	Abbreviation	LOR (g)	PVP (g)	Method of preparation
Raw loratadine	LOR	-	-	-
Physical mixture	PM (1:1)	5	5	Turbula mixer (for 10 mins)
Re-crystallized PM from 100 mL ethanol solution	SE (1:1)	5	5	Solvent evaporation (at 25 °C)
Loratadine-Nanofiber Experiment 1	LOR-NF1	5	5	Electrospinning method (*WD* = 65 mm)
Loratadine-Nanofiber Experiment 2	LOR-NF2	5	5	Electrospinning method (*WD* = 95 mm)

192

193 **2.4 Scanning electron microscopy (SEM)**

194 The morphological appearance of the electrospun fibers was investigated by scanning electron
195 microscopy (SEM) (Hitachi S4700, Hitachi Scientific Ltd., Tokyo, Japan) at 10 kV. The
196 samples were coated with gold-palladium (90 seconds) by a sputter coater (Bio-Rad SC 502,
197 VG Microtech, Uckfield, UK). One hundred nanofibers were selected from each SEM image,
198 and the mean fiber diameter was measured by ImageJ 1.44p software (NIH, USA).
199

200 **2.5 Differential scanning calorimetry (DSC)**

Differential scanning calorimeter (Mettler Toledo TG 821e DSC; Mettler Inc., Schwerzenbach, Switzerland) was used to measure the thermal response of the samples. Approximately 3 – 5 mg of the sample was precisely weighed into DSC sample pans, which were hermetically sealed, then the lid was pierced. Each sample was measured in the temperature interval of 25 °C – 300 °C at a heating rate of 5 °C min^{-1} under constant argon flow of 150 mL min^{-1}.

2.6 Fourier-transform infrared spectroscopy (FT-IR)

FTIR spectrum of each sample was obtained by using Fourier transform infrared spectroscopy (Thermo Nicolet AVATAR 330, USA) equipped with GRAMS/AI Version 7.00 software. The samples were ground with 150 mg dry KBr in a mortar and pestle, then compressed into a disc at 10 t pressure. The discs were scanned 128 times at a resolution of 4 cm^{-1} over 4000-400 cm^{-1} wavenumber region.

2.7 X-ray powder diffraction (XRPD)

The crystalline phase of LOR, PM, SE, and LOR-NFs was characterized using an X-ray powder diffraction (XRPD) BRUKER D8 Advance X-ray diffractometer (Bruker AXS GmbH, Karlsruhe, Germany) with Cu K λ_I radiation (λ = 1.5406 Å) and a VÅNTEC-1 detector. The powder samples were scanned at 40 kV and 40 mA, with an angular range 3° to 40° 2θ, at a step time of 0.1 s and a step size of 0.02°r**.**

Eva software was used to separate the crystal and related amorphous peaks. Thus, the software calculated the values of the integrated intensities of the amorphous and crystalline contribution and the crystalline-only contribution. The crystallinity index values (X_c) of the samples were calculated based on the following equation:

$$Xc = A_{crystalline}/A_{crystalline} + A_{amorphous} \quad (1)$$

2.8 Dissolution studies

Modified paddle method (USP dissolution apparatus, type II Pharma Test, Hainburg, Germany) was used to determine the rates of dissolution of LOR, PM, SE, and LOR-NFs. Samples containing 1.11 mg of loratadine were placed in 100 mL of phosphate buffer solution at pH 7.4. The paddles were rotated at 100 rpm at 37 °C. At predetermined time 5 m aliquot was withdrawn, filtered and measured for loratadine content using UV spectrophotometry (Unicam UV/VIS Spectrophotometer, Cambridge, UK) at λ_{max} 248nm. The sampling was performed for 120 min.

2.9 Model-independent kinetics of dissolution profiles

The dissolution behavior of the samples was characterized by calculating the dissolution efficiency (DE) at different time points. The DE represents the percentage of the ratio of the area up to time t divided by the area that described 100% dissolution at the same time (Khan, 1975):

$$\%DE = (\int_0^t y\ X\ dt)/(y_{100}\ X\ t) \times 100\% \quad (2)$$

The relative dissolution (RD) at 60 min was calculated relative to LOR by using the following formula:

$$RD60\ min = \%\ DE60\ min/\%\ DE60\ min \quad (3)$$

The area under the curve (AUC) was calculated by the trapezoidal method. AUC represents the sum of all trapezia:

$$AUC = \sum_{i=1}^{i=n}[(t_1 - t_{i-1})(y_{i-1} + y_i)/2] \quad (4)$$

Where t_i represents the time point and y_i is the percentage of sample dissolved at time t_i. The mean dissolution time (MDT) was calculated using the following formula (Costa, P., & Lobo, 2001)

$$MDT = \sum_{i-1}^{n} t_{mid} \Delta M / \sum_{i-1}^{n} \Delta M \quad (5)$$

Where i is the dissolution sample number, n is the number of dissolution times, t_{mid} is the time at the midpoint between times t_i and t_{i-1}, and ΔM is the amount of the dissolved drug (mg) between times t_i and t_{i-1}.

3. Results and discussion

3.1 Morphology and diameter of the LOR-NFs

Smooth LOR nanofibers without the presence of beads were obtained from the electrospinning of PVP alcohol solutions (Figure 2c and 2d). The collection distance had a significant effect on the diameter of the prepared nanofibers. 95 mm collection distance resulted in the formation of smooth nanofibers with small diameter (372 ± 181 nm). The low diameter indicates that the nanofibers were stretched enough and sufficiently dried before deposition on the collector. On the other hand, large diameter and fused fibers were obtained at the shorter collection distance (65 mm). The nanofibers in this experiment (LOR-NF1) appeared to not well featured and fused as an indication of the incomplete drying. Furthermore, the protruded fiber shows a large diameter (948 ± 234 nm) and plasticized shape as another indication of not complete drying. The PM showed the characteristic crystal of LOR that showed a crystal size larger than 2 µm (Figure 2a). The SE showed irregular shapes of LOR crystal, both short rod and prisms were present. Moreover, the rod shape crystals exhibited a diameter of 562.7 ± 379 nm. The image of SE (Figure 2b) also showed the aggregation and variety of distribution of LOR within the matrix of PVP polymer.

Figure 2. Scanning electron microscopy images of the **(a)** physical mixture; **(b)** sample prepared by solvent evaporation; **(c)** electrospun nanofibers using the working distance of 65 mm (LOR-NF1); **(d)** electrospun nanofibers using the working distance of 95 mm (LOR-NF2). The SEM image (d) shows separated, more uniform and smaller diameter nanofibers compared to (c).

3.2 Structural analysis (DSC, XRPD, and FT-IR)

The DSC thermogram of LOR exhibited a sharp endothermic peak at 136.65 °C corresponding to its melting point. The filament-forming matrix polymer PVP showed a broad endotherm between 50 and 100 °C with a peak at 90 °C related to dehydration. The PM and SE showed the characteristic peak of LOR indicating the presence of LOR in its crystalline status. However, these endothermic peaks showed a lower intensity compared to pure LOR due to the reduction of crystallinity either by the dilution effect (PM) and/or the preparation method (SE). DSC of LOR-NFs exhibited a broad peak at temperatures lower than 60 °C, primarily caused by the thermal effect of moisture evaporation and also the glass transition. Moreover, the endothermic peak of LOR has disappeared in the prepared NFs indicating that LOR was no longer present as a crystalline, but had been converted into an amorphous state (Figure 3) (Akhgari et al., 2016).

Figure 3. DSC thermograms of the raw materials, reference samples and the prepared nanofibers. The reference samples (PM and SE) show the melting point of LOR while electrospun nanofibers represent the amorphous nature of the LOR.

The X-ray diffraction patterns of the LOR, PVP, PM, LOR-NF1, and LOR-NF2 are presented in Figure 4. LOR showed numerous peaks between 3-30 of the 2-θ scale indicated that LOR is

present as a crystalline material. PVP showed two broad halo peaks specified to amorphous status. PM showed the same characteristic peaks of pure LOR while SE showed the lower intensity of LOR peaks in addition to the absence of many peaks due to the reduction of the crystallinity. LOR-NF1 and LOR-NF2 showed complete disappearance of LOR characteristic peaks. However, the two halo peaks of PVP were observed in the electrospun fibers at the same position and showed the same shape.

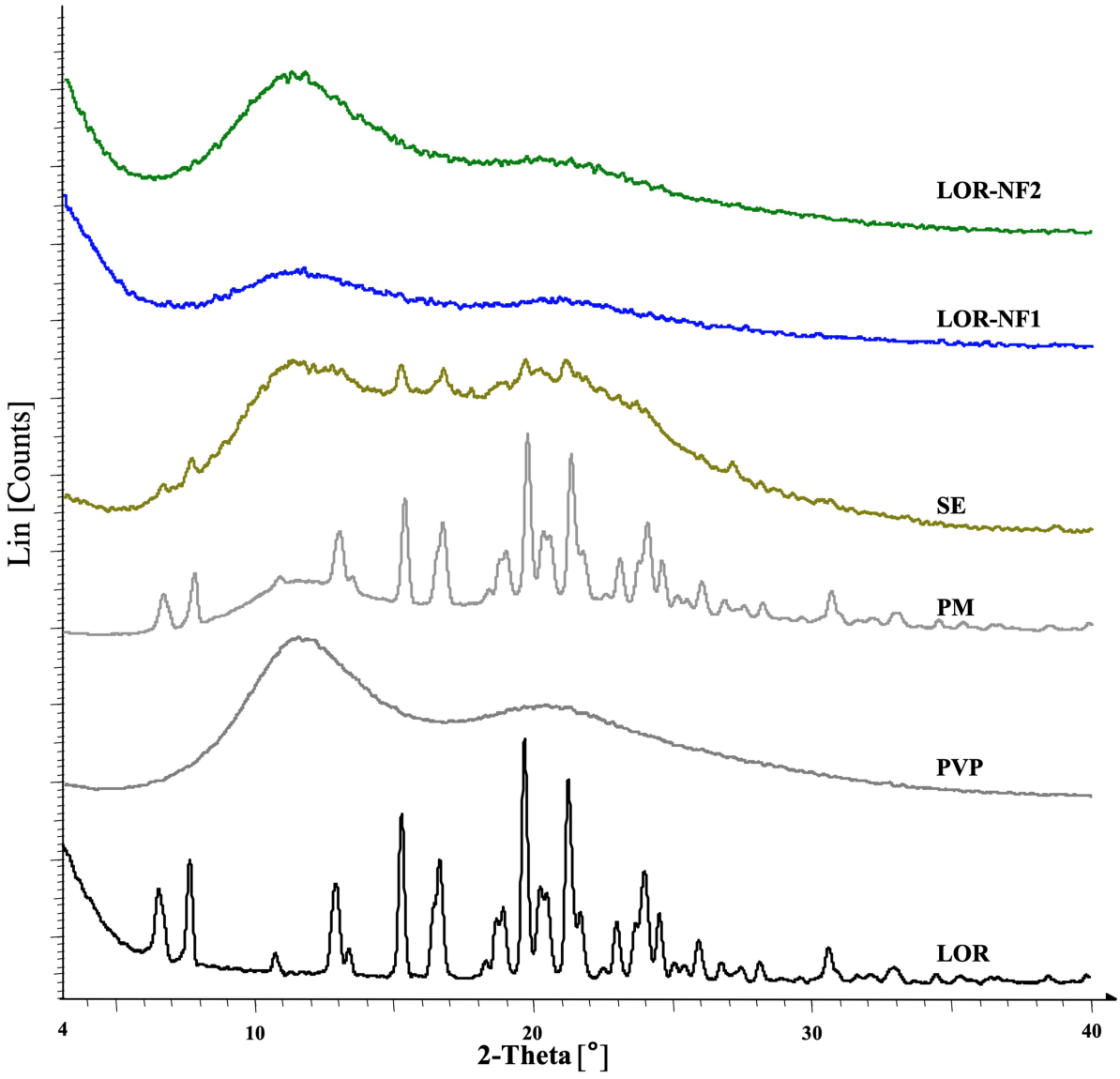

Figure 4. XRPD diffractograms of the raw materials, reference samples and the prepared nanofibers. The electrospun nanofiber samples were amorphous, while the reference samples (PM and SE) show the crystalline peaks of LOR.

The crystallinity index (X_C) values were calculated to reveal the changes in the degree of crystallinity of the LOR nanofibers and SE with respect to the PM (Gombás et al., 2002). The crystallinity indices from XRPD and DSC further suggest the amorphous state of the prepared LOR-NFs (Table 2). The nominal values of X_C obtained from DSC curves were different from that found by XRPD measurements for the samples. The differences in the measurements were expected because of using comparative methods to obtain data rather than absolute ones (Tserki et al., 2006). In the case of XRPD, the XRPD patterns were separated by the software into crystalline and amorphous peaks, and the degree of crystallinity was estimated based on equation (1). In spite of the qualitative analysis of the amorphous peaks by this method, the same procedure was applied to all samples in order to get comparable values. On the other hand, the values obtained by DSC were based on the heat of fusion. Both methods represented the variation of crystallinity between the prepared samples.

Table 2. The calculated crystallinity index (X_c) of the reference samples and the prepared nanofibers after DSC and XRPD measurements compared to LOR.

Sample	**Crystallinity index (%)**	
	XRPD	**DSC**
SE	32.71	47.29
LOR-NF1	30.28	0.93
LOR-NF2	9.79	0.93

FT-IR analysis was performed to check the compatibility and interactions between LOR and the nanofiber matrix (Figure 5). The FTIR bands that are characteristic to LOR are located at 997 cm^{-1} for aryl C-Cl stretching and 1,227cm^{-1} for -C-N stretching of aryl N. In addition to bands at 1560 and 1703 cm^{-1} corresponded to C-O bonds of the amide or ester groups. Bands from 3000 to 2850 cm^{-1} correspond to the C-H bond (Alshweiat et al., 2018). On the other hand, PVP showed its characteristic bands at 3448.3 cm^{-1} due to O-H stretching vibrations, 2924.4 cm^{-1} related to asymmetric stretching of CH_2, 1652.3 cm^{-1} for C=O stretching and a broad peak at 1289.4 cm^{-1} due to C-N stretching vibrations (Sriyanti et al., 2018). The FTIR spectra of the physical mixture and the reference sample showed no obvious shift of the peaks of the functional groups corresponding for hydrogen bonding. However, LOR-NF samples showed shifted peaks of LOR and PVP. The main effects were observed in the O-H and C=O regions. The hydroxyl peak of PVP at 3448.3 cm^{-1} shifted to 3512 cm^{-1} and the C=O stretching peaks at 1652.3 cm^{-1} shifted to 1666.5 cm^{-1}. The band of LOR shifted from 1702.8 to 1666.5 overlapping with the shifted peak of PVP. The peak shift of carbonyl stretching was thought to be a result of hydrogen bond intermolecular interaction between LOR and PVP (Zhao et al., 2017). Since the FTIR results showed only hydrogen bonding, but no covalent bonding, LOR and PVP as nanofibers are indicated to be compatible with each other (Frizon et al., 2013; John et al., 2002).

Figure 5. FT-IR spectra of the raw materials, reference samples and the prepared electrospun nanofibers. The electrospun nanofiber samples and SE sample show an intermolecular interaction between LOR and PVP via hydrogen bond formation.

According to the aforementioned characteristics of the LOR-NFs, only the LOR-NF2 showed the complete separation of the fibers and nanofibers with small diameters. Therefore, it was selected for further solubility and dissolution studies.

3.3 Solubility and Dissolution studies

LOR-NF2 showed a 26.2-fold increase of LOR solubility compared to the pure drug in phosphate buffer solution, pH 7.4. The solubility of LOR-NF2 was 13.1 ± 0.26 μg mL^{-1} compared to 0.50 ± 0.11 μg mL^{-1} for LOR at 25 °C (Table 3). The dissolution behaviors of the samples are shown in Figure 6. LOR-NF2 showed the highest release rate, more than 66% of the drug was released in the first 10 min compared to less than 0.5% of the pure LOR. SE samples also showed higher dissolution than LOR because of their contact with the hydrophilic polymer. However, the PM exhibited a release behavior similar to LOR. The improvement in the dissolution of LOR from the electrospun fibers was attributed to the presence of LOR in the amorphous state. Loratadine has been reported to have higher kinetic energy in the amorphous state, hence higher dissolution than its crystalline state. Moreover, the three-dimensional structure of the electrospun fiber can offer a larger surface area, therefore, water can diffuse more efficiently into the polymer to dissolve the drug. The dissolution efficiency of LOR-NF2 was enhanced at all selected time points, as well as RD value. The mean dissolution time of LOR-NF2 was decreased. These results confirmed that the dissolution became fast due to the amorphous state of the drug in the nanofibers, presence of the additives, and reduction of the particle size Table (4).

Table 3. Solubility (μg mL^{-1}) of LOR and the prepared samples in phosphate buffer at pH 7.4 at a temperature of 25 °C.

Sample	**Solubility (μg mL^{-1})**

LOR	0.50 ± 0.11
PM	6.45 ± 0.06
SE	7.58 ± 0.38
LOR-NF2	13.1 ± 0.11

Figure 6. Dissolution behavior of LOR, reference samples and the prepared electrospun nanofiber with working distance 6.5 mm in phosphate buffer solution, pH 7.4. The nanofiber-based sample has improved dissolution kinetics and higher dissolution rates than the raw LOR or the reference samples (PM and SE).

Table 4. Dissolution efficiency (DE) at different time points, mean dissolution time (MDT), and relative dissolution (RD), with respect to the raw LOR at 60 min of the samples.

Sample	**%DE_{30}**	**%DE_{60}**	**%DE_{120}**	**MDT**	**RD_{60}**
LOR	1.47	3.73	4.60	36.69	-
PM	0.69	1.46	3.45	53.63	0.39
SE	5.64	7.06	8.54	13.28	1.89
LOR-NF2	61.2	70.89	75.52	5.87	19.0

4. Conclusion

This study demonstrated home setup, low-cost, 3D-printed, electrospinning sources for generation of nanofibers using a rotating metal drum as a collector. Nanofibers of LOR were prepared in the hydrophilic PVP polymer and compared to the corresponding physical mixture and conventional reference sample, that was prepared by the solvent evaporation method. The distance between the nozzle and collecting drum was an influential process-parameter; it affected the possibility of preparing separated nanofibers. Moreover, it affected the diameters of the nanofibers. 65 mm distance was optimum to produce separated nanofibers with diameters of 372 nm. The prepared nanofibers displayed an amorphous status of LOR, and the spectroscopic studies indicated interactions between the drug and polymer. As a result of the formation of the amorphous nanofibers, the solubility and dissolution of

LOR were enhanced. Solubility studies showed a marked increase in release rate compared to the pure drug. LOR-NF2 showed a 26.2-fold increase in the solubility of LOR as compared to the pure drug in phosphate buffer solution, pH 7.4. Moreover, more than 66% of the drug was released in the first 10 min compared to less than 4% drug release from the conventional reference sample (SE). Therefore, faster and higher dissolution was achieved for the poorly water-soluble LOR by fabrication of electrospun nanofibers. The improved dissolution could enable the designing of new alternative loratadine formulations, including buccal, transdermal, and topical dosage forms.

Declaration of interests

The authors declare no conflicts of interests.

Authors' contributions

AR designed the experiment and managed the analysis. AA carried out the analysis, interpreted the results, and wrote the manuscript. CI helped in interpreting of the results. GO and AE performed the electrospinning experiments. NR came up with the experimental design and supervised the overall project.

Acknowledgements

The authors would like to thank Jing Huang of The University of Edinburgh for her assistance with the preparation for the experiments. We thank Michel Vong, and Yunxi Gao for their feedback on the paper. We would also like to thank Fergus Dingwall for his appreciated laboratory assistance. The authors acknowledge the Ministry of Human Capacities, Hungary, grant number 20391-3/2018/FEKUSTRAT, for funding.

References

Akhgari, A., Dezfuli, A.G., Rezaei, M., Kiarsi, M., Abbaspour, M., 2016. The design and evaluation of a fast-dissolving drug delivery system for loratadine using the electrospinning method. Jundishapur J. Nat. Pharm. Prod. 11.

https://doi.org/10.17795/jjnpp-33613

Alshweiat, A., Katona, G., Csóka, I., Ambrus, R., 2018. Design and characterization of loratadine nanosuspension prepared by ultrasonic-assisted precipitation. Eur. J. Pharm. Sci. https://doi.org/10.1016/j.ejps.2018.06.010

Ambrus, R., Radacsi, N., Szunyogh, T., van der Heijden, A.E.M., ter Horst, J.H., Szabó-Révész, P., 2013. Analysis of submicron-sized niflumic acid crystals prepared by electrospray crystallization. J. Pharm. Biomed. Anal. 76, 1–7. https://doi.org/10.1016/j.jpba.2012.12.001

Amidon, G.L., Lennernäs, H., Shah, V.P., Crison, J.R., 1995. A Theoretical Basis for a Biopharmaceutic Drug Classification: The Correlation of in Vitro Drug Product Dissolution and in Vivo Bioavailability. Pharm. Res. 12, 413–420. https://doi.org/10.1023/A:1016212804288

Arya, A., Sharma, V., Pathak, K., 2012. Pharmaceutical evaluation and dynamic vapor sorption studies of fast dissolving intraoral films of Loratadine. Pharm. Dev. Technol. 7450, 1–10. https://doi.org/10.3109/10837450.2012.685659

Badawy, S.I.F., Ghorab, M.M., Adeyeye, C.M., 1996. Characterization and bioavailability of danazol-hydroxypropyl β-cyclodextrin coprecipitates. Int. J. Pharm. 128 128, 45–54.

Baskakova, A., Awwad, S., Gill, H., Khaw, P.T., Brocchini, S., Zhilyakova, E., Williams, G.R., Hospital, M.E., 2016. Electrospun formulations of acyclovir , ciprofloxacin and cyanocobalamin for ocular drug delivery. Int. J. Pharm. 502, 208–228.

Brewster, M.E., Verreck, G., Chun, I., Rosenblatt, J., Mensch, J., Dijck, A. Van, Noppe, M., Arie, A., 2004. The use of polymer-based electrospun nanofibers containing amorphous drug dispersions for the delivery of poorly water-soluble pharmaceuticals.

Chuangchote, S., Sagawa, T., Yoshikawa, S., 2009. Electrospinning of Poly (vinyl pyrrolidone): Effects of Solvents on Electrospinnability for the Fabrication of Poly (p -

442 phenylene vinylene) and TiO 2 Nanofibers. J. Appl. Polym. Sci. 114, 2777–2791.
443 https://doi.org/DOI 10.1002/app.30637
444 Costa, P., & Lobo, J.M.S., 2001. Modelling and Comparison of Dissolution Profiles. Eur. J.
445 Pharm. Sci. 13, 123–133. https://doi.org/10.1016/S0928-0987(01)00095-1
446 Craig, D.Q.M., 2002. The mechanisms of drug release from solid dispersions in water-soluble
447 polymers. Int. J. Pharm. https://doi.org/10.1016/S0378-5173(01)00891-2
448 Dagenais, C., Avdeef, A., Tsinman, O., Dudley, A., Beliveau, R., 2009. P-glycoprotein
449 deficient mouse in situ blood-brain barrier permeability and its prediction using an in
450 combo PAMPA model. Eur. J. Pharm. Sci. 38, 121–137.
451 https://doi.org/10.1016/j.ejps.2009.06.009
452 Fong, H., Chun, I., Reneker, D.H., 1999. Beaded nanofibers formed during electrospinning.
453 Polym. 40 1585–4592.
454 Frizon, F., Eloy, J. de O., Donaduzzi, C.M., Mitsui, M.L., Marchetti, J.M., 2013. Dissolution
455 rate enhancement of loratadine in polyvinylpyrrolidone K-30 solid dispersions by solvent
456 methods. Powder Technol. 235, 532–539. https://doi.org/10.1016/j.powtec.2012.10.019
457 Gombás, Á., Szabó-Révész, P., Kata, M., Regdon, G., Eros, I., 2002. Quantitative
458 determination of crystallinity of α-lactose monohydrate by DSC. J. Therm. Anal.
459 Calorim. 68, 503–510. https://doi.org/10.1023/A:1016039819247
460 Han, M.Z.I.K., Aus, D.R., Filipovi, P., 2004. Classification of Loratadine Based on the
461 Biopharmaceutics Drug Classification Concept and Possible in Vitro – in Vivo
462 Correlation. Biol. Pharm. Bull 27, 1630–1635. https://doi.org/10.1248/bpb.27.1630
463 Huang, J., Radacsi, N., 2019. Low-cost FDM 3D-printed modular
464 electrospray/electrospinning setup for biomedical applications. 3D Print. Med.
465 Submitted, 2019.
466 Huang, Z.M., Zhang, Y.Z., Kotaki, M., Ramakrishna, S., 2003. A review on polymer

467 nanofibers by electrospinning and their applications in nanocomposites. Compos. Sci.
468 Technol. 63, 2223–2253. https://doi.org/10.1016/S0266-3538(03)00178-7
469 Jiang, H., Fang, D., Hsiao, B., Chu, B., Chen, W., 2004. Preparation and characterization of
470 ibuprofen-loaded poly(lactide-co-glycolide)/poly(ethylene glycol)-g-chitosan electrospun
471 membranes. J. Biomater. Sci. Polym. Ed. 15, 279–296.
472 John, J., Mani, R., Bhattacharya, M., 2002. Evaluation of compatibility and properties of
473 biodegradable polyester blends. J. Polym. Sci. Part A Polym. Chem. 40, 2003–2014.
474 https://doi.org/10.1002/pola.10297
475 Khan, K.A., 1975. The concept of dissolution efficiency. J. Pharm. Pharmacol. 27, 48–49.
476 https://doi.org/10.1111/j.2042-7158.1975.tb09378.x
477 Li, D., Xia, Y., 2003. Fabrication of Titania Nanofibers by Electrospinning. Nano Lett. 3,
478 554–560.
479 Li, H., Tan, Y., Yang, L., Gao, L., Wang, T., Yang, X., Quan, D., 2015. Dissolution
480 evaluation in vitro and bioavailability in vivo of self-microemulsifying drug delivery
481 systems for pH-sensitive drug loratadine. J. Microencapsul. 32, 175–180.
482 https://doi.org/10.3109/02652048.2014.985340
483 Li, X., Kanjwal, M.A., Lin, L., Chronakis, I.S., 2013. Electrospun polyvinyl-alcohol
484 nanofibers as oral fast-dissolving delivery system of caffeine and riboflavin. Colloids
485 Surfaces B Biointerfaces 103, 182–188. https://doi.org/10.1016/j.colsurfb.2012.10.016
486 Nacsa, Á., Ambrus, R., Berkesi, O., Szabó-Révész, P., Aigner, Z., 2008. Water-soluble
487 loratadine inclusion complex: Analytical control of the preparation by microwave
488 irradiation. J. Pharm. Biomed. Anal. 48, 1020–1023.
489 https://doi.org/10.1016/j.jpba.2008.07.001
490 Nacsa, Á., Berkesi, O., Szabó-Révész, P., Aigner, Z., 2009. Achievement of pH-independence
491 of poorly-soluble, ionizable loratadine by inclusion complex formation with dimethyl-ß-

cyclodextrin. J. Incl. Phenom. Macrocycl. Chem. 64, 249–254. https://doi.org/10.1007/s10847-009-9558-1

Nagy, Z.K., Balogh, A., Démuth, B., Pataki, H., Vigh, T., Szabó, B., Molnár, K., Schmidt, B.T., Horák, P., Marosi, G., Verreck, G., Van Assche, I., Brewster, M.E., 2015. High speed electrospinning for scaled-up production of amorphous solid dispersion of itraconazole. Int. J. Pharm. 480, 137–142. https://doi.org/10.1016/j.ijpharm.2015.01.025

Nagy, Z.K., Balogh, A., Vajna, B., Farkas, A., Patyi, G., Kramarics, Á., Marosi, G., 2012. Comparison of Electrospun and Extruded Soluplus®-Based Solid Dosage Forms of Improved Dissolution. J. Pharm. Sci. 101, 322–332. https://doi.org/10.1002/jps.22731

Nuansing, W., Ninmuang, S., Jarernboon, W., Maensiri, S., Seraphin, S., 2006. Structural characterization and morphology of electrospun TiO2nanofibers. Mater. Sci. Eng. B Solid-State Mater. Adv. Technol. 131, 147–155. https://doi.org/10.1016/j.mseb.2006.04.030

Omar, L., El-Barghouthi, M.I., Masoud, N.A., Abdoh, A.A., Al Omari, M.M., Zughul, M.B., Badwan, A.A., 2007. Inclusion complexation of loratadine with natural and modified cyclodextrins: Phase solubility and thermodynamic studies. J. Solution Chem. 36, 605–616. https://doi.org/10.1007/s10953-007-9136-3

Paaver, U., Laidmäe, I., Santos, H.A., Yliruusi, J., 2016. Development of a novel electrospun nanofibrous delivery system for poorly water-soluble β -sitosterol. Asian J. Pharm. Sci. 11, 500–506. https://doi.org/10.1016/j.ajps.2016.04.005

Potrč, T., Baumgartner, S., Roškar, R., Planinšek, O., Lavrič, Z., Kristl, J., Kocbek, P., 2015. Electrospun polycaprolactone nanofibers as a potential oromucosal delivery system for poorly water-soluble drugs. Eur. J. Pharm. Sci. 75, 101–113. https://doi.org/10.1016/j.ejps.2015.04.004

Radacsi, N., Campos, F.D., Chisholm, C.R.I., Giapis, K.P., 2018. Spontaneous formation of

517 nanoparticles on electrospun nanofibres. Nat. Commun. 9, 3–10.
518 https://doi.org/10.1038/s41467-018-07243-5
519 Radacsi, N., Giapis, K.P., Ovari, G., Szabó-Révész, P., Ambrus, R., 2019. Electrospun
520 nanofiber-based niflumic acid capsules with superior physicochemical properties. J.
521 Pharm. Biomed. Anal. 166, 371–378. https://doi.org/10.1016/j.jpba.2019.01.037
522 Rodriguez Amado, J.R., Prada, A.L., Duarte, J.L., Keita, H., da Silva, H.R., Ferreira, A.M.,
523 Sosa, E.H., Carvalho, J.C.T., 2017. Development, stability and in vitro delivery profile of
524 new loratadine-loaded nanoparticles. Saudi Pharm. J. 25, 1158–1168.
525 https://doi.org/10.1016/j.jsps.2017.07.008
526 Ryu, Y.J., Kim, H.Y., Lee, K.H., Park, H.C., Lee, D.R., 2003. Transport properties of
527 electrospun nylon 6 nonwoven mats. Eur. Polym. J. 39, 1883–1889.
528 https://doi.org/10.1016/S0014-3057(03)00096-X
529 Shahriar, S., Mondal, J., Hasan, M., Revuri, V., Lee, D., Lee, Y.-K., 2019. Electrospinning
530 Nanofibers for Therapeutics Delivery. Nanomaterials 9, 532.
531 https://doi.org/10.3390/nano9040532
532 Simons, F.E.R., 2002. Comparative pharmacology of H1 antihistamines: clinical relevance.
533 Am. J. Med. 113 Suppl, 38S–46S. https://doi.org/10.1016/S0002-9343(02)01436-5
534 Sriyanti, I., Edikresnha, D., Rahma, A., Munir, M.M., Rachmawati, H., Khairurrijal, K., 2018.
535 Mangosteen pericarp extract embedded in electrospun PVP nanofiber mats:
536 Physicochemical properties and release mechanism of α-mangostin. Int. J. Nanomedicine
537 13, 4927–4941. https://doi.org/10.2147/IJN.S167670
538 Tserki, V., Matzinos, P., Pavlidou, E., Vachliotis, D., Panayiotou, C., 2006. Biodegradable
539 aliphatic polyesters . Part I . Properties and biodegradation of poly (butylene succinate-
540 co -butylene adipate) 91. https://doi.org/10.1016/j.polymdegradstab.2005.04.035
541 Verreck, G., Chun, I., Peeters, J., Rosenblatt, J., Brewster, M.E., 2003. Preparation and

characterization of nanofibers containing amorphous drug dispersions generated by electrostatic spinning. Pharm. Res. 20, 810–817. https://doi.org/10.1023/A:1023450006281

Yang, Q., Zhenyu, L.I., Hong, Y., Zhao, Y., Qiu, S., Wang, C.E., Wei, Y., 2004. Influence of solvents on the formation of ultrathin uniform poly(vinyl pyrrolidone) nanofibers with electrospinning. J. Polym. Sci. Part B Polym. Phys. 42, 3721–3726. https://doi.org/10.1002/polb.20222

Yu, D., Branford-White, C., White, K., Li, X.-L., Zhu, L.-M., 2010. Dissolution Improvement of Electrospun Nanofiber-Based Solid Dispersions for Acetaminophen. AAPS PharmSciTech 11, 809–817. https://doi.org/10.1208/s12249-010-9438-4

Yu, D.G., Branford-White, C., Shen, X.X., Zhang, X.F., Zhu, L.M., 2010. Solid dispersions of ketoprofen in drug-loaded electrospun nanofibers. J. Dispers. Sci. Technol. 31, 902–908. https://doi.org/10.1080/01932690903223948

Zhao, Y., Song, X., Sun, J., He, Z., Sun, M., Zhang, S., Wang, J., 2017. Molecular mechanism of polymer-assisting supersaturation of poorly water-soluble loratadine based on experimental observations and molecular dynamic simulations. Drug Deliv. Transl. Res. 7, 738–749. https://doi.org/10.1007/s13346-017-0401-8